DETERMINATION OF LINE-OF-SIGHT INTEGRATED HEAT RELEASE RATE FLUCTUATIONS IN PULSATED FLAMES BY LASER INTERFEROMETRIC VIBROMETRY

J. Li[*], D. Durox[*], F. Richecoeur[*], T. Leitgeb[**], F. Giuliani[**], T. Schuller[*]

Jingxuan.li@em2c.ecp.fr

* Laboratoire EM2C, CNRS and Ecole Centrale Paris, 92295 Châtenay-Malabry, France.

** Institute for Thermal Turbomachinery and Machine Dynamics, Graz University of Technology, 8010 Graz, Austria.

Abstract

An optical technique is proposed to obtain quantitative estimates of heat release rate fluctuations in flames submitted to flow modulations. The diagnostic relies on the determination of density fluctuations integrated in the line-of-sight along a laser beam crossing the flame and impinging on a fixed mirror. A Laser Interferometric Vibrometer (LIV) is used to determine fluctuations in the reflected speckle signal and determine time resolved density fluctuations. It is shown that these density fluctuations in the flame region result mainly from perturbations in the heat release rate. The technique is validated in the case of pulsated laminar premixed flames. Measurements are compared to line-of-sight integrated chemiluminescence emission data collected with a CCD camera. A good agreement is obtained for harmonic flow modulations at different forcing frequencies and perturbation levels. This work validates the principle of this alternative technique and lays the foundations for future developments towards more practical configurations.

1 Introduction

The heat release rate is one fundamental quantity in combustion which is difficult to measure in practical systems except in a few generic cases. This paper aims at developing a simple technique to obtain quantitative time resolved estimates of heat release rate fluctuations. The principle of the technique is presented together with experimental validations for generic premixed flames submitted to flow modulations.

Heat release rate is generally estimated from the chemiluminescence emission of the flame or by using more sophisticated diagnostics based on laser-induced fluorescence. Recording the natural emission of the flame is the simplest technique yielding time-resolved information and is widely used to infer perturbations in the global heat release rate by collecting the total emission from the flame. The chemiluminescence emission from naturally excited radicals formed within the flame front, such as OH^*, CH^* and C_2^*, is often considered as a good marker of heat release rate [1, 2]. This is generally admitted in premixed flames in absence of mixture composition inhomogeneities. However, subsequent analysis showed that the emission of these radicals may also depend on the turbulence intensity [3, 4], flame strain rate [3, 5, 6], flame front curvature [7], local mixture composition [5], temperature and pressure [8, 9, 10, 11]. Measurements are then often limited to flame images for qualitative analysis except in a few studies where the signal is calibrated using specific post-processing procedures to recover the heat release rate [12, 13, 14]. Laser induced fluorescence (LIF) can also be envisaged to obtain quantitative estimates of the heat release rate (see for example [3, 15]). LIF is however heavy to implement and require high power well-tuned laser beams at different wavelengths. LIF

has been tested yet only in well controlled generic steady configurations. Time resolved data are more difficult to obtain due to the limited repetition rates from the lasers and the limited energy delivered per pulse. One advantage is to obtain space resolved data in the laser sheet whereas chemiluminescence generally yields a line-of-sight integrated information that can eventually be deconvoluted if the flame symmetry is cylindrical (see for example [16]). Local chemiluminescence measurements can be obtained as well but are more rare [17, 18]. The development of alternative techniques to obtain time resolved heat release rate measurements when the reactants are not perfectly mixed is an active field of investigation.

The objective of this study is to present one solution based on laser homodyne interferometry to determine heat release rate fluctuations. This technique is relatively simple to implement and yields quantitative time resolved data which are in principle not limited to perfectly premixed combustion modes. The different applications targeted are turbulent combustion modeling, analysis of flame dynamics, characterization of combustion noise and control of acoustic induced combustion instabilities. The principle of the method is described and first experimental validations in well controlled generic configurations are presented. This method is based on the determination of flow density fluctuations integrated along the optical path of a laser beam crossing a flame and reflected by a mirror. When the flame is wrinkled due for example to a self-sustained oscillation [19] or when it is submitted to flow modulations [20], this produces perturbations in the heat release rate which are accompanied by large density fluctuations in the reaction zone [21] constituting important sound sources that radiate combustion noise [12]:

$$\frac{\partial \rho'}{\partial t} = \frac{1}{\bar{c}^2}\frac{\partial p'}{\partial t} - \frac{\gamma - 1}{\bar{c}^2}\dot{q}' \tag{1}$$

where the density, pressure, speed of sound, specific heat capacities ratio and heat release rate per unit volume are represented by ρ, p, c, γ and $\dot{q}$, respectively. The mean and fluctuating components are denoted by the superscripts ($^-$) and ($'$). This expression is a simplified version for density fluctuations comprising acoustic and entropic contributions that are dominated by heat release rate disturbances in air combustion systems [21, 22]. The contribution of acoustic disturbances can generally neglected compared to entropy fluctuations in reacting flows and this enables to link heat release rate fluctuations directly to the density perturbations. This type of approximation has for example been used in analysis of combustion noise [23]. It constitutes an interesting alternative to access to heat release rate fluctuations. Experimental validations have however not been envisaged yet.

Laser interferometry has already been envisaged to determine density and density fluctuations in turbulent non reacting flows [24, 25] as well as in perturbed reacting flows [26]. This technique yields a line-of-sight integrated measurement of the refractive index n which is linked to density ρ by the Gladstone-Dale relation :

$$n - 1 = G\rho \tag{2}$$

where G denotes the Glastone-Dale constant. Density disturbances in the flow thus manifest in changes of refractive index [24, 25] leading to perturbations of the phase signal φ measured by an interferometer between a laser beam crossing the flame and a reference beam :

$$\varphi(x, y, t) = \frac{2\pi}{\lambda_0}\int_{\text{object}} n(x, y, z, t)\mathrm{d}z - \frac{2\pi}{\lambda_0}\int_{\text{reference}} n(x, y, z, t)\mathrm{d}z \tag{3}$$

where λ_0 denotes the laser wavelength. When the geometrical path of laser is kept constant, the phase lag φ between the two beams is directly linked to density changes integrated along the optical path [25, 26].

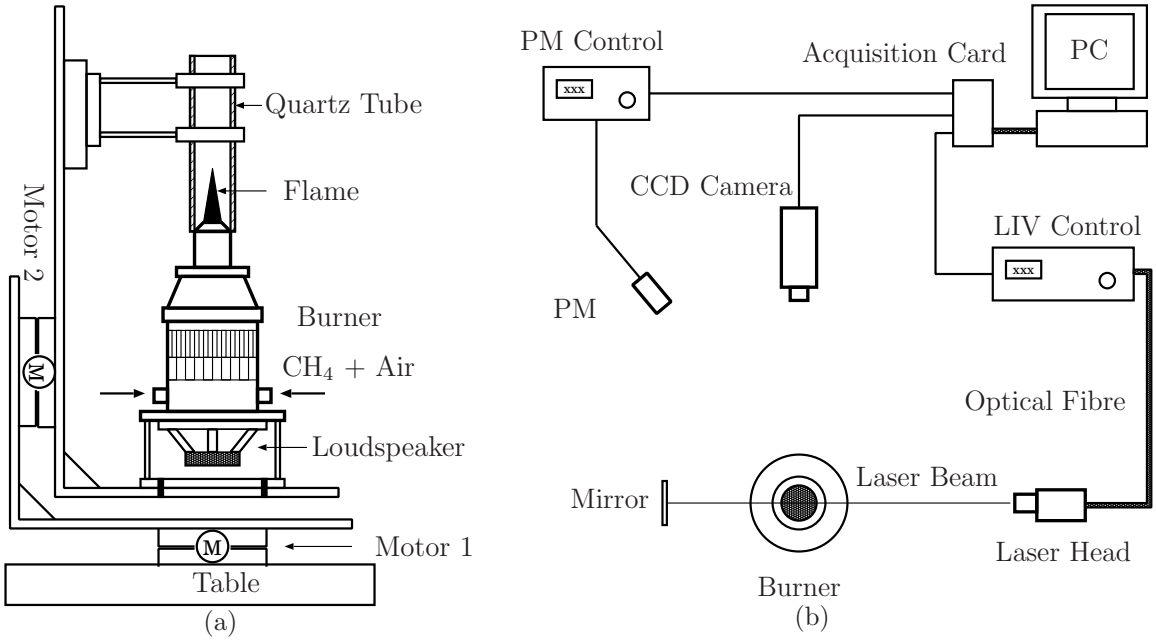

Figure 1: Schematic of the setup. (a) Burner fixed on a two axes micrometric displacement table; (b) Arrangement of the measurement devices.

The experimental configuration used to validate theoretical predictions is presented in section 2. The different diagnostics are described together with the main elements of the Laser Interferometric Vibrometer (LIV) system used in this study. Comparisons between measurements are presented in section 3. Correlations are successively established between line-of-sight integrated chemiluminescence emission disturbances measured by a CCD camera and the signal from the LIV for conical flames submitted to flow modulations at different frequencies and forcing levels. Concluding remarks are made in the last section.

2 Experimental arrangement

Measurements are conducted on an axisymmetric burner with a $D = 20$ mm outlet nozzle diameter shown in Fig. 1(a). Laminar conical premixed methane/air flames can be stabilized on the lips of the burner and are submitted to velocity modulation by a loudspeaker fixed at the base of the burner. The burner is also fixed on a two axes micrometric displacement table to move the burner in the vertical and horizontal directions by increments of 1 μm. The steady and r.m.s axial velocity components are measured with a hot-wire probe placed at the burner outlet when the flow is modulated (in absence of combustion).

A quartz tube can be added on the top of the burner to confine the flame. This is used to avoid perturbations of the interface between burned gases and ambient air. In presence of flow disturbances this interface responds with the same frequency as the flame modulation in the absence of flame tube or when it is partially confined. This phenomenon can be identified in the color Schlieren images obtained for a conical premixed flame submitted to a flow velocity modulation with a frequency of $f = 50.1$ Hz presented in Fig. 2. The flame is in this case partially confined by a quartz tube placed on the top to reduce buoyancy effects. Red and green filters are used in these experiments to separate the light deflected in different horizontal directions and highlight the flame front from the limit of the hot plume with ambient air [27]. The comparison between the two images indicates a motion of the hot plume boundary accompanying the deformation of the flame front. Consequences on the resulting line-of-sight integrated signal resulting from the rate

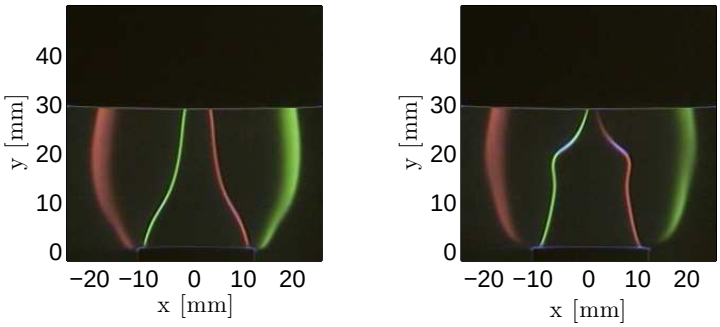

(a) (b)

Figure 2: Two snapshots of color Schlieren images highlighting the instantaneous locations of the flame front and burned gases boundary when the flame is submitted to a harmonic velocity modulation at $f = 50.1$ Hz with an amplitude level $v_{urms}/\bar{v}_u = 0.14$. Flow operating conditions : $\phi = 1.0$, $\bar{v}_u = 1.5$ m s^{-1}.

of change of density fluctuations measured at different positions within the flame by LIV are rapidly described in Fig. 3. The time resolved recorded signals enable a spectral analysis. The different power spectra (PSD) show that the rate of change of density is altered greatly around the flame with a peak frequency corresponding to the modulation frequency. Positions within the flame are indicated by the cartesian coordinates [x,y] in millimeters, where x corresponds to the radial distance with respect to the burner axis and y is the height above the burner outlet. By focusing on the PSD level at the modulation frequency $f = 50$ Hz, one can find in Fig. 3 that the rate of change of density at the position [16,15] corresponding to boundary of the hot plume, oscillates with about the same amplitude as that at the position [8,15] corresponding to the location of the flame front. The rate of change of density near the boundary region of the hot plume can be illustrated by mapping the value of the PSD peak at $f = 50$ Hz in Fig. 4. It is clear that the interface between the burned gases and ambient air corresponds to a region with

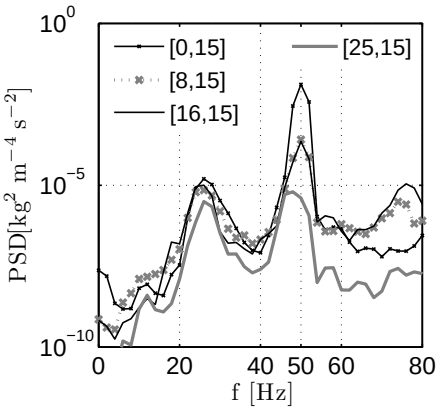

Figure 3: Power Spectra Density (PSD) analysis of the rate of change of density deduced from LIV at four positions [x,y]=[0,15], [8,15], [16,15] and [25,15] where the radial x and axial y distances are given in millimeters.

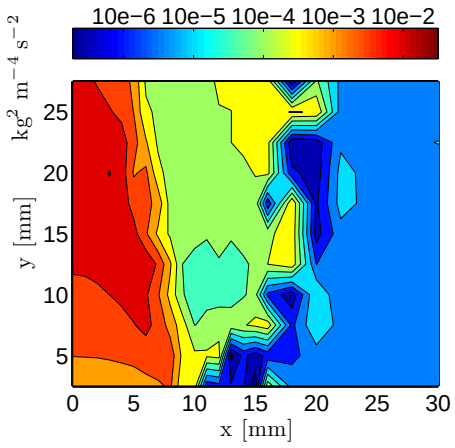

Figure 4: Contour plot of the PSD peak value at $f = 50$ Hz of the rate of change of density deduced from LIV measured of half the flame imaged in Fig. 2.

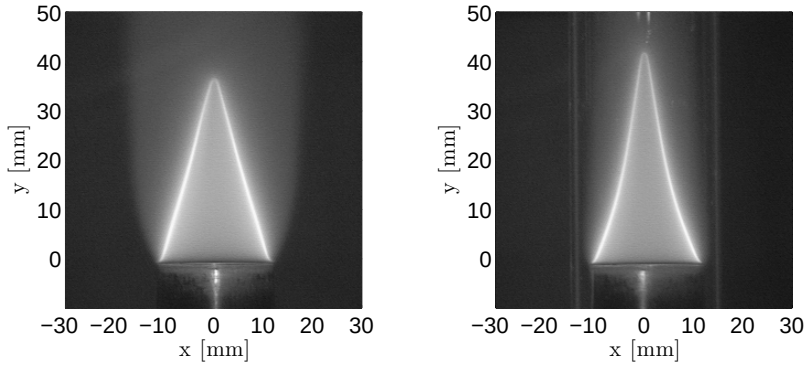

(a) without tube (b) with tube

Figure 5: Steady flame in the absence of quartz tube (left, flame height $H = 37$ mm) and with quartz tube (right, flame height $H = 42$ mm). Flow operating conditions: $\phi = 1.00$, $\bar{v}_u = 1.5$ m s^{-1}.

relatively large rate of change of density and constitutes a source of disturbances to infer heat release rate perturbations.

To avoid this problem, a quartz tube of 150 mm long with an inner diameter of 27 mm is used to confine the flame. The burned gases are in this case directly in contact with the quartz. The axis of quartz tube is aligned with the burner axis and the bottom of the quartz tube in contact with the burner is sealed to avoid entrainment of external air. The shape of one steady flame together with the quartz tube is shown in Fig. 5. The conical shape of the flame is slightly bent due to the pressure of the burned gases acting on the flame and causing a vertical acceleration of the gases in the centerline [28]. The flame height is stretched from 37 mm in absence of confined tube to 42 mm with the tube. These conditions are obtained for a flow velocity $\bar{v}_u = 1.5$ m s^{-1} and a stoichiometric mixture $\phi = 1.00$ corresponding to a thermal power of 1.1 kW.

Snapshots of the pulsated flame are recorded by a CCD camera equipped with an electronic shutter to set the exposure time to 1/2000 s. The camera acquisition rate is 1 frame per second, while the forcing frequencies driving the loudspeaker are chosen as 50.1 Hz and 100.1 Hz. These parameters enable to record 10 frames per modulation

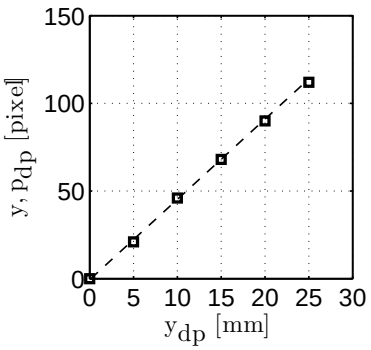

Figure 6: Plot of the pixel displacement in CCD images (unit: pixel) versus flame displacement imposed by the micrometric system(unit: mm).

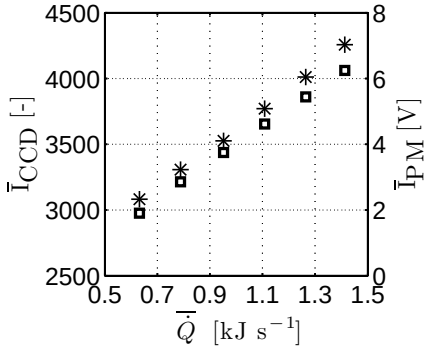

Figure 7: Plots of summation of $\bar{I}$ of all pixels recorded by CCD camera (marker $\square$) and PM (marker $*$) versus $\bar{\dot{Q}}$.

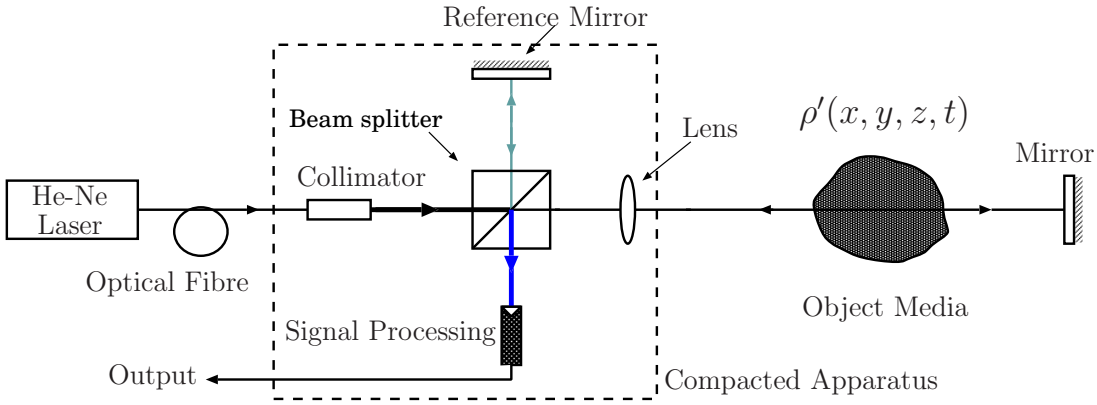

Figure 8: Schematic view of the principle of Laser Interferometric Vibrometer.

period. The focus of the camera is well adjusted to the size of the flame and images are digitized with a matrix of 288 pixels×384 pixels. The CCD is equipped with square pixels corresponding to an aspect ratio of unity. The micrometric displacement table is used to calibrate the flame images that can be translated in the focal plane by known displacements as illustrated in Fig. 6 yielding 1 mm for 4.52 pixels.

For well premixed flame in absence of mixture composition inhomogeneities, perturbations in the chemiluminescence intensity I of free radicals OH*, C_2* or CH* present in the flame front are proportional to heat release rate disturbances [2, 27]:

$$\dot{Q} = kI \tag{4}$$

where k is constant for a given equivalence ratio ϕ and experimental setup. In this paper, a photomultiplier (PM) and the CCD camera are both employed to record the chemiluminescence intensity from the flame. The PM featuring a large solid angle yields a global integrated signal, while the camera gives a line-of-sight integrated information. Each pixel from the color image of the CCD camera is converted to a double precision number measuring the total light intensity cumulated on the pixel. The summation of the values of all pixels in the image yields the global the light intensity I_{CCD} measured by the camera. This quantity can be compared to the light intensity I_{PM} recorded by the PM. By modifying the flow velocity at the burner outlet, it is possible to examine the evolutions of the signals I_{PM} and I_{CCD} as a function of the heat release rate calculated $\overline{\dot{Q}} = \rho_u \bar{v}_u S \Delta q$, where ρ_u denotes the density of the fresh mixture, $S = \pi D^2/4$ the surface area of the nozzle outlet, Δq the heat release per unit mass of mixture and $\bar{v}_u$ the flow velocity determined from the massflow controller indications (Fig. 7). The coefficient k_{CCD} and k_{PM} appearing in equation (4) can then be determined and used to obtain quantitative estimates of heat release rate from the PM and camera signals.

In these experiments a LIV model LS-V 2500 from SIOS Meβtechnik GmbH is used to determine line-of-sight integrated density fluctuations around the flame (Fig. 1(b)). It comprises a He-Ne laser ($\lambda_0 = 633$ nm) with an object beam traversing a sensor head constituted by a compact objective used both as a transmitter and receiver. The laser passes through the reacting flow and is then reflected by a flat aluminum mirror, passes through the reacting flow again and is recorded by the sensor head. The distance between the sensor head and burner axis is fixed to $L_{bl} = 500$ mm and $L_{bm} = 200$ mm between the mirror and burner axis. The laser is focused on the mirror and the laser beam in the flame zone does not exceed 2 mm in these experiments.

The schematic of the main components of this system is shown in Fig. 8 [26]. This type of device is commonly used in vibration analysis to characterize surface oscillations

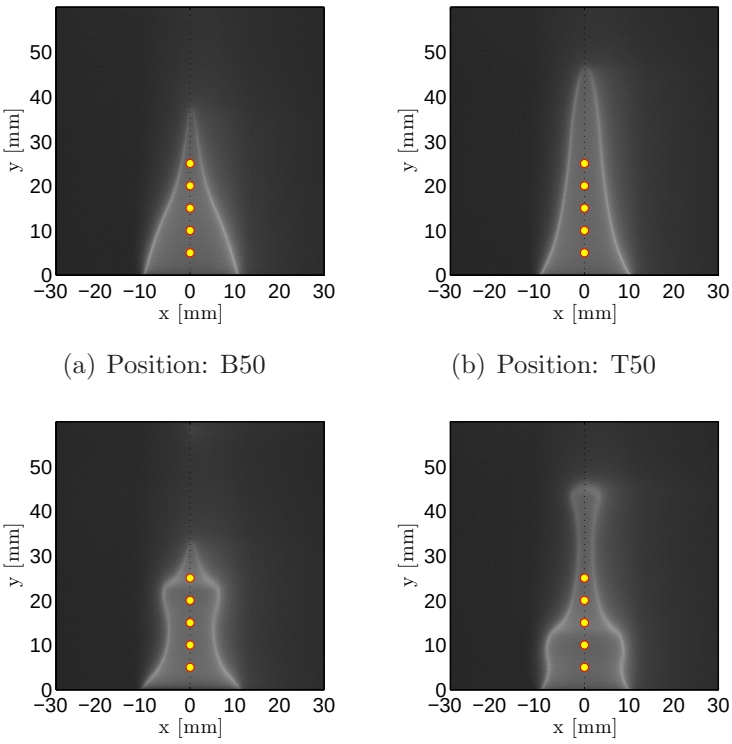

(a) Position: B50 (b) Position: T50

(c) Position: B100 (d) Position: T100

Figure 9: Snapshots of modulated flames at two forcing frequencies and same the perturbation amplitude. (a) and (b): f=50.1 Hz, $v_{urms}/\bar{v}_u$=0.14; (c) and (d): f=100.1 Hz, $v_{urms}/\bar{v}_u$=0.14. The four images correspond to different instants in the modulation cycle emphasized by the red circles in Fig. 10. The five yellow disks in these images correspond to the measurement locations. Flow operating conditions: $\bar{v}_u = 1.5$ m s^{-1} and $\phi = 1.00$.

when the beam crosses a uniform medium characterized by a constant refractive index. In this case equation (3) can be simplified to :

$$\varphi(t) = \frac{4\pi}{\lambda_0} z'(t) \tag{5}$$

where, $z'(t)$ denotes the surface displacement equal to half of the optical path length change. For our purpose the geometrical beam path L is kept constant, it is then possible to detect density fluctuations altering the optical path by delaying or advancing the phase lag between incident and reflected beams. Equation (3) yields in this case :

$$\varphi(t) = \frac{4\pi G}{\lambda_0} \int_L \rho'(z,t) dz = \frac{4\pi G}{\lambda_0} < \rho'(t) > L \tag{6}$$

where $< \rho'(t) >$ corresponds to the resulting density fluctuation along the geometrical path L. The voltage output from the LIV signal processor yields an information on the distance $z'(t)$ which is proportional to density fluctuations integrated along the beam of light. The link between these quantities can be obtained by the combination of equations (5) and (6):

$$\text{Output} = k_{gain} z'(t) = k_{gain} G < \rho'(t) > L \tag{7}$$

where k_{gain} is the unit conversion factor ranging from 0.24 μm V^{-1} to 990.44 μm V^{-1}. The Glastone-Dale constant is equal to $G = 2.5\,10^{-4}$ kg m^{-3} $\pm$ 3% for CH_4-air mixture [26].

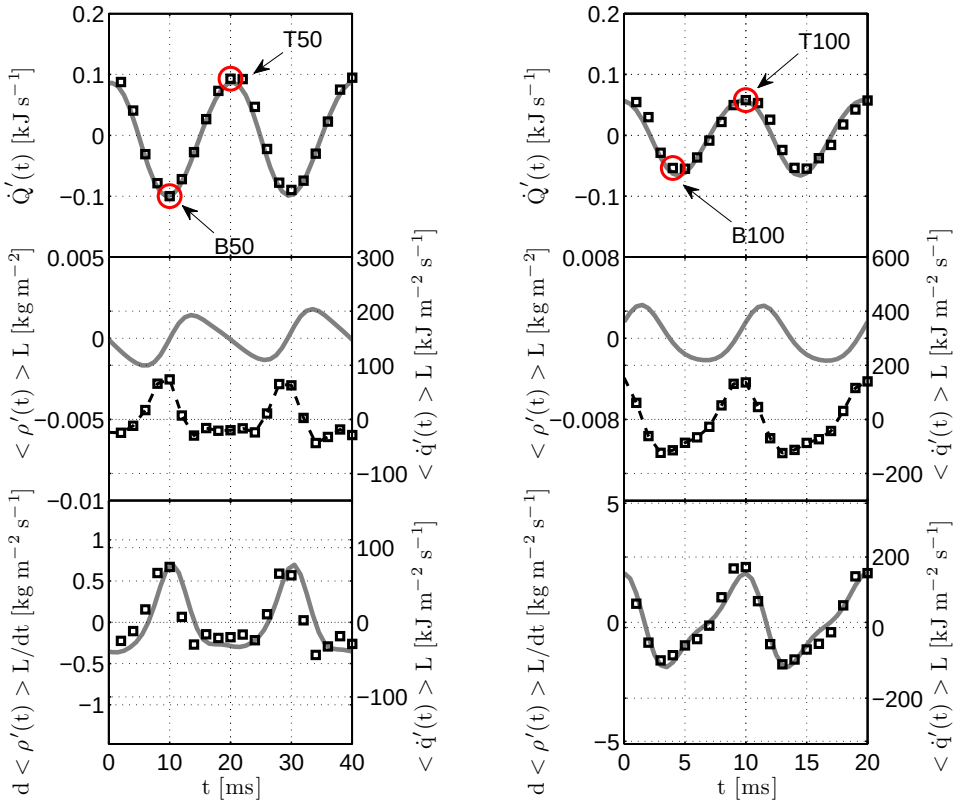

(a) f=50.1 Hz, $v_{urms}/\bar{v}_u$=0.14.

(b) f=100.1 Hz, $v_{urms}/\bar{v}_u$=0.14.

Figure 10: Measurements at $y = 15$ mm for a moderate perturbation level. Top: time-history comparison between heat release rate perturbations determined with the PM (continuous line) and with the CCD camera (markers). Middle : comparison between $< \rho'(t) > L$ (continuous line) and $< \dot{q}'(t) > L$ (markers). Bottom: comparison between $\mathrm{d} < \rho'(t) > L/\mathrm{d}t$ (continuous line) and $< \dot{q}'(t) > L$ (markers).

The frequency passband from the LIV ranges from 0 to 500 kHz to detect disturbances in density at very high frequencies. The system is limited by its maximum translation rate $[\mathrm{d}z'(t)/\mathrm{d}t]_{\max} = 1.5$ m s^{-1} yielding the corresponding value $[\mathrm{d} < \rho'(t) > L/\mathrm{d}t]_{max}$ = 6000 kg m^{-2} s^{-1} for the rate of change of line-of-sight integrated density fluctuations which is much bigger than the values concerned in this paper.

3 Results and discussion

Measurements are presented for a stoichiometry conical flame modulated at two frequencies $f = 50.1$ Hz and $f = 100.1$ Hz with different perturbation levels. The amplitude is determined in a separate set of experiments in absence of combustion with a hot wire placed at the burner outlet but under the same flow conditions. The shutter speed of the camera is set to 1/2000 s to obtain sharp images. The frame acquisition rate cannot be adjusted in the CCD camera and is fixed to 1 frame/s which enables to record 10 frames per modulation period for the two forcing frequencies considered here $f = 50.1$ and 100.1 Hz, yielding an equivalent sampling rate of 501 Hz and 1001 Hz respectively. 400 continuous images are recorded for each operating conditions enabling to sort the images and reconstruct the evolution of flame motion at each phase in the modulation cycle. The signals from of the LIV and the PM are recorded and sampled at a frequency of 8192 Hz over a period of 1 second. These signals are then filtered by a low-pass zero-

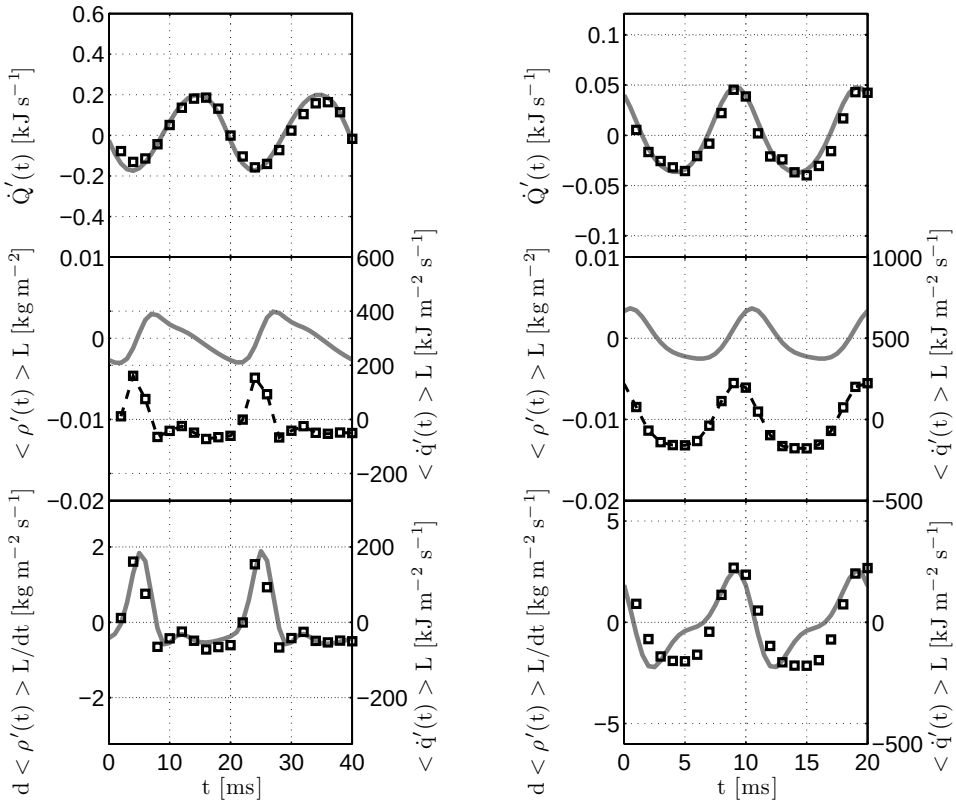

(a) f=50.1 Hz, $v_{urms}/\bar{v}_u$=0.28. (b) f=100.1 Hz, $v_{urms}/\bar{v}_u$=0.21.

Figure 11: Measurements at y = 15 mm at a higher perturbation level. Top: time-history comparison between heat release rate perturbations determined with the PM (continuous line) and with the CCD camera (markers). Middle : comparison between $< \rho'(t) > L$ (continuous line) and $< \dot{q}'(t) > L$ (markers). Bottom: comparison between d $< \rho'(t) > L$/dt (continuous line) and $< \dot{q}'(t) > L$ (markers).

phase shift filter with a cut-off frequency equal to 400 Hz. LIV measurement and flame images records with the CCD camera are done in separate experiments. The PM signal is then used as a reference to synchronize the signals from LIV and CCD camera.

Figure 9 shows instantaneous views of the flame modulated at two frequencies with a constant amplitude $v_{urms}/\bar{v}_u$=0.14. The left two images feature smaller deformations of the flame front than the right two images during the oscillation cycle. Larger deformations of the flame shape induce larger heat release rate perturbations as shown in the top graphs in Fig. 10. The resulting heat release rate perturbations determined from the PM and CCD signals are correlated to find the phase difference between these devices and synchronize all the diagnostics. LIV measurements are carried out at five different heights above the burner from 5 mm to 25 mm separated by 5 mm increments along the burner axis which are indicated in Fig. 9 by 5 spots.

The line-of-sight integrated heat release rate perturbation $< \dot{q}'(t) > L$ is determined by integrating the pixel values of the CCD cameras on a matrix of 9 pixels × 9 pixels located around the measurement position to take into account the finite width of the laser beam which has a diameter of 2 mm. The signal $< \dot{q}'(t) > L$ together with the line-of-sight integrated density fluctuations $< \rho'(t) > L$ are plotted in the middle graphs in Fig. 10 for a moderate perturbation level $v_{urms}/\bar{v}_u$=0.14. It is more interesting to compare the time evolution of the time derivative of $< \rho'(t) > L$ and the signal $< \dot{q}'(t) > L$ represented

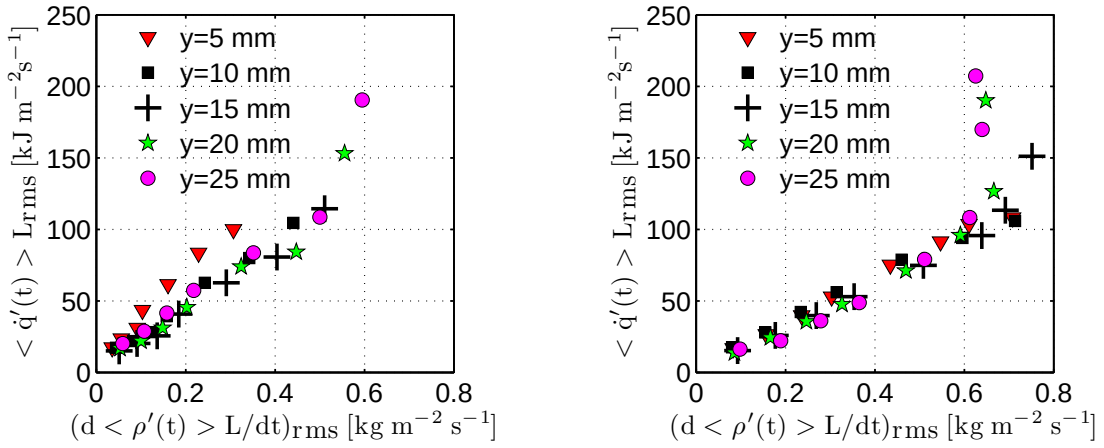

(a) f=50.1 Hz, $v_{urms}/\bar{v}_u$ varies from 0.03 to 0.35. (b) f=100.1 Hz, $v_{urms}/\bar{v}_u$ varies from 0.02 to 0.21.

Figure 12: Plots of the r.m.s value of integrated heat release rate signal $< \dot{q}'(t) > L$ as function of the time derivative of line-of-sight integrated density fluctuation d$< \rho'(t) > L$/dt.

in the bottom graphs in Fig. 10. A perfect match between the two signals can be found both at low $f = 50.1$ Hz and high $f = 100.1$ Hz frequencies at this moderate perturbation level confirming the validity of equation (1).

Increasing the modulation amplitude, the shapes of the four signals $\dot{Q}'(t)$, $< \dot{q}'(t) > L$, $< \rho'(t) > L$ and d$< \rho'(t) > L$/dt feature larger differences with pure harmonic responses in Fig. 11. A spectral analysis not presented here shows that the main oscillation peak is still clearly associated with the modulation frequency for all cases investigated. A good correlation between the signals $< \dot{q}'(t) > L$ and d$< \rho'(t) > L$/dt can still be noted even at high forcing amplitude $v_{urms}/\bar{v}_u$=0.28 for the low frequency $f = 50.1$ Hz. The two signals at a higher forcing frequency $f = 100.1$ Hz slightly deviate with a small phase lag. The correlation between the two signals deteriorate at the lowest positions in the measurements at $y = 5$ mm. This is accompanied by a phase difference which is not shown here. In the vicinity of the burner outlet the flame is not perfectly confined and this may cause the slight deviations observed. The link between the two signals $< \dot{q}'(t) > L$ and d$< \rho'(t) > L$/dt can directly be examined by plotting the r.m.s values of the two signals for the different measurement locations and the different modulation amplitudes investigated. Results presented in Fig. 12 for the two modulation frequencies explored clearly validate the linear link between these two signals. Data collapse on a single line which is not function of the measurement position within the flame, except for the case measured at $y = 5$ mm where the flame may not be fully confined. A saturation phenomenon occurs however at high modulation amplitudes and the slope also depends on the modulation frequency. This last phenomenon is probably due to the finite width of the laser beam which is not so small compared to the perturbation wavelength along the flame front at 100.1 Hz.

Conclusions

It has been shown that it is possible to estimate heat release rate disturbances by measuring density fluctuations in modulated flames. This has led to line-of-sight integrated measurements of density fluctuations along the optical path passing through the flame determined with a Laser Interferometric Vibrometer. Experimental validations were carried

out on a generic configuration with a stoichiometric premixed conical flame submitted to harmonic flow modulations. Estimates of heat release rate fluctuations deduced from LIV were compared with data obtained from the chemiluminescence emission of the flame. A good correlation has been found between the two techniques at different forcing frequencies and modulation amplitudes. A proportional relation between the two signals was found that does not depend on the measurement position, but is affected by the modulation frequency. Validation of this alternative technique must be conducted in different combustion modes.

Acknowledgement

Jingxuan Li is supported by a doctoral fellowship from China Scholarship Council, Project 111, Grant No. B08009.

References

[1] Hurle, I. R., Price, R. B., Sugden, T. M., and Thomas, A., 1968. "Sound Emission from Open Turbulent Premixed Flames". *Royal Society of London Proceedings Series A,* ***303***, Mar., pp. 409–427.

[2] Price, R., Hurle, I., and Sugden, T., 1969. "Optical studies of the generation of noise in turbulent flames". *Symposium (International) on Combustion,* ***12***(1), pp. 1093 – 1102.

[3] Ayoola, B., Balachandran, R., Frank, J., Mastorakos, E., and Kaminski, C., 2006. "Spatially resolved heat release rate measurements in turbulent premixed flames". *Combust. Flame,* ***144***(1-2), pp. 1 – 16.

[4] Lauer, M., and Sattelmayer, T., 2010. "On the adequacy of chemiluminescence as a measure for heat release in turbulent flames with mixture gradients". *J. Eng. Gas Turbines Power,* ***132***, p. 061502 (8 pages).

[5] Hardalupas, Y., and Orain, M., 2004. "Local measurements of the time-dependent heat release rate and equivalence ratio using chemiluminescent emission from a flame". *Combust. Flame,* ***139***(3), pp. 188 – 207.

[6] Nori, V. N., and Seitzman, J. M., 2009. "CH* chemiluminescence modeling for combustion diagnostics". *Proc. Combust. Inst.,* ***32***(1), pp. 895 – 903.

[7] Najm, H. N., Paul, P. H., Mueller, C. J., and Wyckoff, P. S., 1998. "On the adequacy of certain experimental observables as measurements of flame burning rate". *Combust. Flame,* ***113***(3), pp. 312 – 332.

[8] Higgins, B., McQuay, M. Q., Lacas, F., and Candel, S., 2001. "An experimental study on the effect of pressure and strain rate on ch chemiluminescence of premixed fuel-lean methane/air flames". *Fuel,* ***80***(11), pp. 1583 – 1591.

[9] Docquier, N., Belhalfaoui, S., Lacas, F., Darabiha, N., and Rolon, C., 2000. "Experimental and numerical study of chemiluminescence in methane/air high-pressure flames for active control applications". *Proc. Combust. Inst.,* ***28***(2), pp. 1765 – 1774.

[10] Ikeda, Y., Kojima, J., and Hashimoto, H., 2002. "Local chemiluminescence spectra measurements in a high-pressure laminar methane/air premixed flame". *Proc. Combust. Inst.,* ***29***(2), pp. 1495 – 1501.

[11] Kim, J.-R., Akamatsu, F., Choi, G.-M., and Kim, D.-J., 2009. "Observation of local heat release rate with changing combustor pressure in the CH4/air flame (wrinkled laminar regime)". *Thermochimica Acta,* ***491***(1-2), pp. 109 – 115.

[12] Schuller, T., Durox, D., and Candel, S., 2002. "Dynamics of and noise radiated by a perturbed impinging premixed jet flame". *Combust. Flame,* ***128***(1-2), pp. 88–110.

[13] Tran, N., Ducruix, S., and Schuller, T., 2009. "Damping combustion instabilities with perforates at the premixer inlet of a swirled burner". *Proc. Combust. Inst.,* ***32***, pp. 2917–2924.

[14] Palies, P., Durox, D., Schuller, T., and Candel, S., 2010. "The combined dynamics of swirler and turbulent premixed swirling flames". *Combust. Flame,* ***157***, pp. 1698–1717.

[15] Fayoux, A., Zähringer, K., Gicquel, O., and Rolon, J., 2005. "Experimental and numerical determination of heat release in counterflow premixed laminar flames". *Proc. Combust. Inst.,* ***30***(1), pp. 251 – 257.

[16] G. Herding, R. Snyder, C. R., and Candel, S., 1998. "Investigation of cryogenic propellant flames using computerized tomography of oh emission images". *J. Propuls Power,* ***13***, pp. 146–151.

[17] Kojima, J., Ikeda, Y., and Nakajima, T., 2000. "Spatially resolved measurement of OH*, CH*, and C2* chemiluminescence in the reaction zone of laminar methane/air premixed flames". *Proc. Combust. Inst.,* ***28***(2), pp. 1757 – 1764.

[18] Kojima, J., Ikeda, Y., and Nakajima, T., 2005. "Basic aspects of OH(A), CH(A), and C2(d) chemiluminescence in the reaction zone of laminar methane-air premixed flames". *Combust. Flame,* ***140***(1-2), pp. 34 – 45.

[19] Candel, S., 2002. "Combustion dynamics and control: Progress and challenges". *Proc. Combust. Inst.,* ***29***(1), pp. 1 – 28.

[20] Ducruix, S., Thierry, S., Durox, D., and Candel, S., 2003. "Combustion dynamics and instabilities: Elementary coupling and driving mechanisms". *J. Propuls Power,* ***19***(5), pp. 722–734.

[21] Candel, S., Durox, D., Ducruix, S., Birbaud, A.-L., Noiray, N., and Schuller, T., 2009. "Flame dynamics and combustion noise: progress and challenges". *International Journal of Aeroacoustics,* ***8***(1), pp. 1–56.

[22] Dowling, A. P., 1995. "The calculation of thermoacoustic oscillations". *J. Sound Vibration,* ***180***(4), pp. 557 – 581.

[23] Ihme, M., Pitsch, H., and Bodony, D., 2009. "Radiation of noise in turbulent non-premixed flames". *Proc. Combust. Inst.,* ***32***(1), pp. 1545 – 1553.

[24] Mayrhofer, N., and Woisetschläger, J., 2001. "Frequency analysis of turbulent compressible flows by laser vibrometry". *Exp. Fluids,* ***31***, pp. 153–161.

[25] Köberl, S., Fontaneto, F., Giuliani, F., and Woisetschläger, J., 2010. "Frequency-resolved interferometric measurement of local density fluctuations for turbulent combustion analysis". *Meas.Sci.Technol.,* ***21***(3), p. 035302.

[26] Giuliani, F., Leitgeb, T., Lang, A., and Woisetschläger, J., 2010. "Mapping the density fluctuations in a pulsed air-methane flame using laser-vibrometry". *J. Eng. Gas Turbines Power,* ***132***(3), p. 031603.

[27] Ducruix, S., Durox, D., and Candel, S., 2000. "Theoretical and experimental determinations of the transfer function of a laminar premixed flame". *Proc. Combust. Inst.,* ***28***(1), pp. 765 – 773.

[28] Higuera, F., 2009. "Aerodynamics of a slender axisymmetric bunsen flame with large gas expansion". *Combust. Flame,* ***156***(5), pp. 1063 – 1067.